research papers

Characteristics of Friedel pairs and diffraction contrast tomography with non-perpendicular rotation axis

Qiru Yi,[a] Gang Li,[a]* Jie Zhang,[a] Sheng-Nian Luo,[b] Duan Fan,[b] Zhenhua Gao,[a] Yanping Wang,[a] Guanfeng Gao,[c] Shiping Jiang[c] and Xiaoming Jiang[a]

[a]Institute of High Energy Physics, Chinese Academy of Science, Yuquan Road 19B, Shijingshan District, Beijing, People's Republic of China, [b]The Peac Institute of Multiscale Science, 2nd Eastern Section Chuanda Road, Chengdu, Sichuan, People's Republic of China, and [c]University of Science and Technology of China, 96 Jinzhai Road, Baohe District, Hefei, Anhui, People's Republic of China. *Correspondence e-mail: lig@ihep.ac.cn

The characteristics of Friedel pairs in diffraction contrast tomography (DCT) are studied in the condition that the rotation axis of the sample is not exactly perpendicular to the incident X-ray direction. For the rotation axis approximately aligned along the vertical direction, the Friedel pairs close to the horizontal plane are insensitive to the non-perpendicularity of the rotation axis, and can be used to refine the sample-to-detector distance and X-ray energy, while the Friedel pairs close to the vertical direction are sensitive to the non-perpendicularity of the rotation axis, and can be used to determine the rotation axis orientation. The correct matching proportion of Friedel pairs decreases with increasing non-perpendicularity of the rotation axis. A method of data processing considering rotation axis misalignment is proposed, which significantly increases the correct matching and indexing proportions of the diffraction spots. A pure aluminium polycrystalline sample is investigated using DCT at beamline 4W1A of Beijing Synchrotron Radiation Facility. Based on the analysis of Friedel pairs, the sample-to-detector distance and X-ray energy are refined to be 8.67 mm and 20.04 keV, respectively. The non-perpendicular angle of the rotation axis is calculated to be 0.10°. With these refined geometric parameters, the matching proportion of the spatial position of diffraction spots is 90.62%. Three-dimensional reconstruction of the sample with 13 grains is realised using the algebraic reconstruction technique. It is demonstrated that the precise correction of the orientation of the sample rotation axis is effective in DCT suffering from rotation axis misalignment, and the higher accuracy in determining the rotation axis is expected to improve the reconstruction precision of grains.

1. Introduction

As a kind of three-dimensional (3D) X-ray diffraction technique, X-ray diffraction contrast tomography (DCT) is a non-destructive imaging method which can yield grain-level microstructures of polycrystalline materials in three dimensions (Ludwig *et al.*, 2008; Johnson *et al.*, 2008). It can obtain the grain boundary crystallographic planes and orientation distribution function of polycrystalline materials (Ludwig *et al.*, 2010; King *et al.*, 2010; Kostenko *et al.*, 2012; Syha *et al.*, 2012; Reischig *et al.*, 2013). Reconstruction of grains is performed using the 3D algebraic reconstruction technique (ART) combining with extinction spots and diffraction spots (Johnson *et al.*, 2008). For materials with negligible intra-granular orientation spread the reconstruction precision of DCT is comparable to that of electron backscatter diffraction (Syha *et al.*, 2013). Along with the propagation-based X-ray
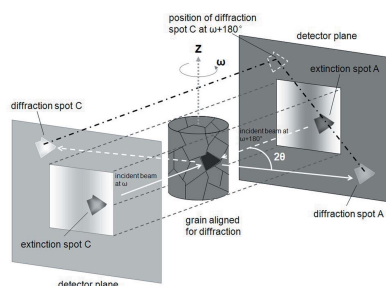
phase-contrast imaging (Cloetens *et al.*, 1997), DCT is applied to the studies of crack growth and fatigue damage of polycrystalline materials (King *et al.*, 2008; Ludwig *et al.*, 2009a; Herbig *et al.*, 2011; King *et al.*, 2011) and recently extended to neutron imaging (Peetermans & Lehmann, 2013).

The 3D X-ray diffraction technique can be divided into near- and far-field approaches. A number of software packages for indexing grains which are applicable to the diffraction data have been developed (Lauridsen *et al.*, 2001; Schmidt, 2005, 2014; Suter *et al.*, 2006; Moscicki *et al.*, 2009; Bernier *et al.*, 2011; Sharma *et al.*, 2012 Li *et al.*, 2013). In the near-field case, the spatial and angular information are coupled in diffraction spots and scattering vectors cannot be derived from the diffraction spots directly (Nervo *et al.*, 2014). There are two types of solutions to resolve the ambiguity: (i) forward modeling (Schmidt, 2005; Suter *et al.*, 2006; Li *et al.*, 2013), (ii) tricks to determine the scattering vectors from near-field data by means of ray-tracing on multiple detectors (Lauridsen *et al.*, 2001) or the use of Friedel pairs (Ludwig *et al.*, 2009b). DCT is a variant of near-field 3DXRD. The method of using Friedel pairs for DCT data processing and geometry refinement has been applied under the condition that the rotation axis has high orientation precision of better than 0.01°(Ludwig *et al.*, 2009b; Reischig *et al.*, 2013). However, perfect alignment of the rotation axis can hardly be achieved in experiments; a small non-perpendicularity of the rotation axis may affect the correct matching of Friedel pairs, thus undermining the 3D reconstruction of grains. This article mainly studies the characteristics of Friedel pairs in the case of low precision in the rotation axis orientation, as well as the correct matching proportions of Friedel pairs at different non-perpendicularities of the rotation axis and sampling angular intervals. It is found that the effect of rotation axis non-perpendicularity varies with the orientations of lattice planes, and that the correct matching proportion of Friedel pairs is severely reduced by rotation axis inclination. We demonstrate that it is possible to accurately determine the inclination of the rotation axis and to match and index near-field diffraction data suffering from rotation axis misalignment. We introduce a modified calibration and indexing procedure, based on the analysis of a subset of the available Friedel pairs, and successfully apply this procedure to experimental data of an aluminum polycrystalline sample with a non-perpendicular rotation axis. Some limitations of this approach are discussed.

2. Principle of Friedel pairs

The principle of DCT data processing based on Friedel pairs is shown in Fig. 1. During the experiment, the sample is continuously rotated by 360°, and the diffraction contribution will be observed when the Bragg condition is fulfilled. If the rotation axis is perpendicular to the incident beam, the diffraction contribution will be observed both in ω and $\omega +$ 180° corresponding to the Bragg reflections from (hkl) and ($-h-k-l$). Such pairs are called Friedel pairs. In a full 360° rotation, each set of lattice planes can give rise to four diffraction contributions at most (Ludwig *et al.*, 2009b).
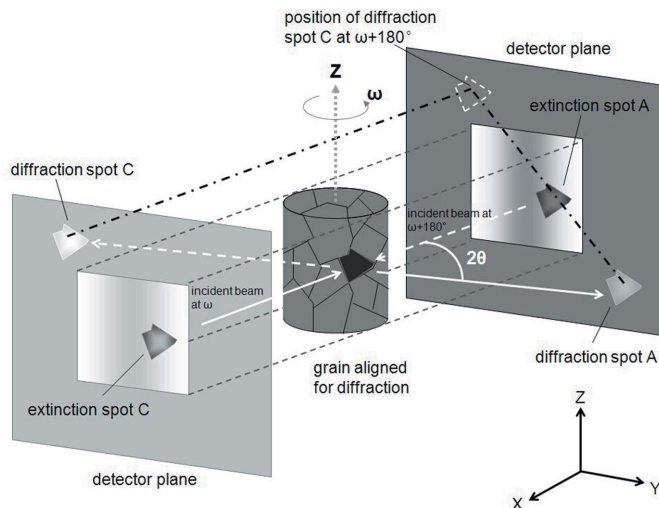
Figure 1
Schematic of a Friedel pair in the coordinate system fixed to the sample. In the condition that the rotation axis is perpendicular to the incident beam, a Friedel pair consisting of diffraction spots A and C appears at ω and $\omega +$ 180° (Ludwig *et al.*, 2009b).

However, when the rotation axis is not precisely perpendicular to the incident beam, the characteristics of the Friedel pairs will be different, as discussed below.

The laboratory coordinate system is also shown in Fig. 1. The X axis is parallel to the incident beam, and the Z axis is vertical in this work.

3. Characteristics of Friedel pairs in the non-perpendicular rotation axis condition

When diffraction from (hkl) lattice planes with a Bragg angle θ appears at a rotation angle ω, the angle between the normal vector of the (hkl) lattice plane and the negative direction of the incident beam is $\varphi = 90° - \theta$. If the rotation axis is perpendicular to the incident beam, the diffraction arising from ($-h-k-l$) will appear at $\omega +$ 180° with $\varphi = 90° + \theta$ as shown in Fig. 2(a). However, when the rotation axis is not perpendicular to the incident beam, the angle between the Friedel pair will not equal 180° as shown in Fig. 2(b).

We assume that the unit vector of the rotation axis is $\mathbf{r} = (r_x, r_y, r_z)$, and the unit vector of the normal of the (hkl) lattice plane is $\mathbf{a} = (a_x, a_y, a_z)$. We can obtain $\mathbf{a}_{\text{rot}}$ *via* rotating $\mathbf{a}$ by ω using Rodrigues' rotation formula:

$$\mathbf{a}_{\text{rot}} = \mathbf{a} \cos \omega + (\mathbf{r} \times \mathbf{a}) \sin \omega + \mathbf{r}(\mathbf{r} \cdot \mathbf{a})(1 - \cos \omega), \quad (1)$$

$\mathbf{a}_{\text{rot}} = (a_x, a_y, a_z) \times$

$$\begin{bmatrix} r_x^2(1 - \cos \omega) + \cos \omega & r_x r_y(1 - \cos \omega) + r_z \sin \omega & r_x r_z(1 - \cos \omega) - r_y \sin \omega \\ r_y r_x(1 - \cos \omega) - r_z \sin \omega & r_y^2(1 - \cos \omega) + \cos \omega & r_y r_z(1 - \cos \omega) + r_x \sin \omega \\ r_z r_x(1 - \cos \omega) + r_y \sin \omega & r_z r_y(1 - \cos \omega) - r_x \sin \omega & r_z^2(1 - \cos \omega) + \cos \omega \end{bmatrix}$$

$$(2)$$

Assuming that the vector (1, 0, 0) is the negative direction of the incident beam and the angle between $\mathbf{a}_{\text{rot}}$ and (1, 0, 0) is φ, we then have

(a)

(b)
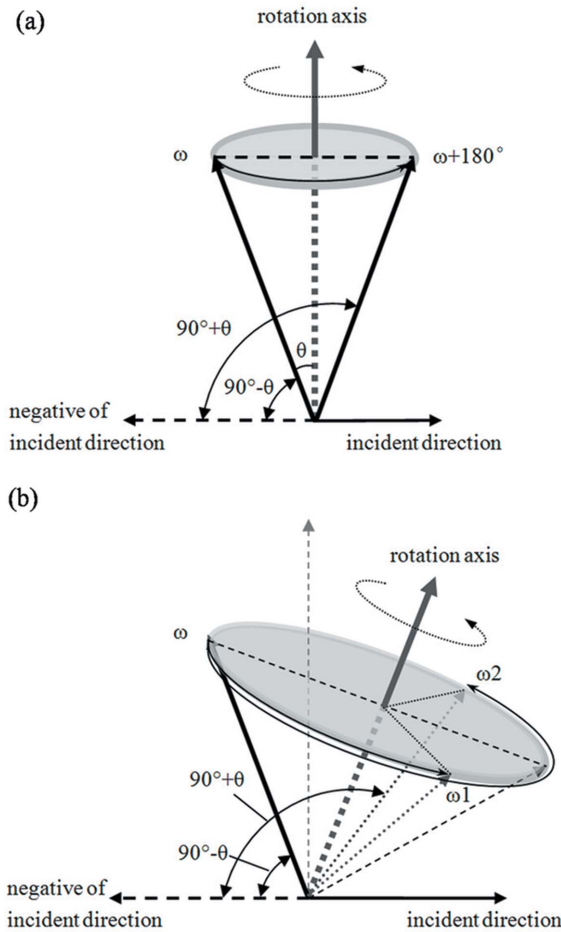
Figure 2
Sketches of Friedel pairs for different rotation axes. (*a*) The rotation axis is perpendicular to the incident direction. The diffraction spot and its pair appearing at ω and $\omega + 180°$ correspond to the angle between the normal vector of the (*hkl*) lattice plane and the negative of the incident direction being equal to $90° - \theta$ and $90° + \theta$, respectively. (*b*) The pair of the diffraction spots appearing at ω do not appear at $\omega + 180°$ when the rotation axis is inclined.

$$\cos \varphi = \frac{\mathbf{a}_{\mathrm{rot}} \cdot (1, 0, 0)}{\left| \mathbf{a}_{\mathrm{rot}} \right|}. \tag{3}$$

We can obtain equation (4) based on equations (2) and (3),

$$\cos \varphi = \left(a_x r_x^2 + a_y r_y r_x + a_z r_z r_x \right)(1 - \cos \omega) + a_x \cos \omega - \left(a_y r_z - a_z r_y \right) \sin \omega. \tag{4}$$

When φ is equal to $90° - \theta$ or $90° + \theta$, diffraction will be observed. From a Friedel pair, we acquire two groups of φ, ω and $\mathbf{a}(a_x, a_y, a_z)$, and then substitute them into equation (4) to obtain two equations. Combining with $|\mathbf{r}| = 1$, we can obtain the unit vector of the rotation axis $\mathbf{r}(r_x, r_y, r_z)$. The Friedel pair can be chosen according to the following discussions.

3.1. Friedel pairs from (*nh nk nl*) lattice planes

The (*nh nk nl*) lattice planes ($n = 1, 2, \dots$) have the same normal vector but different Bragg angles. When the rotation axis is perpendicular to the incident beam with a precision of better than $0.01°$, we can ignore the deflection of the rotation

axis (Reischig *et al.*, 2013). Here we assume the rotation axis has a deflection of $0.01°$ in the XZ plane, and the unit vector of the rotation axis is $r = [\sin(0.01°), 0, \cos(0.01°)]$. In a full $360°$ rotation, the angular interval of ω is $0.01°$. We take the normal vector of the (*nh nk nl*) lattice planes $\mathbf{a} = [\sin(25°), 0, \cos(25°)]$ as an example. Using equation (4), we can obtain the φ (ω) curve as shown in Fig. 3, where the maximum value of φ is $114.98°$, and the minimum value is $65°$. The diffraction is observed when φ is equal to $90° - \theta$ or $90° + \theta$. As shown in Fig. 3, A–C and B–D are two Friedel pairs when the Bragg angle is $10°$. The number of diffractions varies if we change the Bragg angle as shown in Table 1.

We consider the case that four diffractions can be observed, and different Bragg angles correspond to different values of $\omega_C - \omega_A$. $\Delta\omega$ is used to represent the angle difference between $\omega_C - \omega_A$ and $180°$, and its values for different Bragg angles θ are displayed in Table 2.
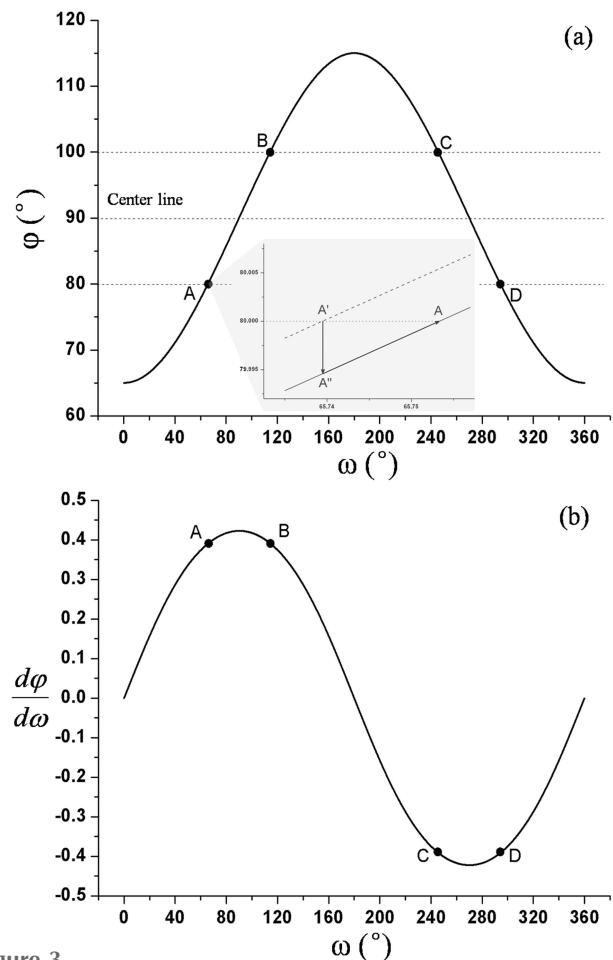
Figure 3
φ (ω) (*a*) and its gradient (*b*) with the rotation axis tilted by an angle of $0.01°$ on the XZ plane. A, B, C and D denote diffraction spots. Spot A on the φ (ω) curve has been magnified to help explain the movement of this spot from A$'$ on the curve of perfect alignment (dashed line) to A. When the rotation axis is tilted by $0.01°$ in the XZ plane, the φ (ω) curve as shown by the dashed line will move down to the position of the solid line (if the tilted angle is $-0.01°$, the curve will move up) and A$'$ moves to A$''$. In order to maintain the Bragg condition, A$''$ has to ascend along the curve to A.

Table 1
Number of diffractions related to different Bragg angles.

Bragg angle	$\varphi = 90° - \theta$	$\varphi = 90° + \theta$	No. of diffractions
$\theta > 25°$	$< 65°$	$> 115°$	0
$\theta = 25°$	$65°$	$115°$	1
$24.98° < \theta < 25°$	$65° < \varphi < 65.02°$	$114.98° < \varphi < 115°$	2
$\theta = 24.98°$	$65.02°$	$114.98°$	3
$\theta < 24.98°$	$> 65.02°$	$< 114.98°$	4

Table 2
Rotation angles of Friedel pair A–C and angle difference $\Delta\omega$ for different Bragg angles.

Bragg angle (θ)	Rotation angle (A)	Rotation angle (C)	$\Delta\omega$
1°	87.66°	267.62°	0.04°
4°	80.53°	260.48°	0.05°
8°	70.80°	250.75°	0.05°
12°	60.55°	240.50°	0.05°
16°	49.31°	229.25°	0.06°
20°	35.99°	215.92°	0.07°
24°	15.77°	195.61°	0.16°

It can be seen from Table 2 that, for different lattice planes with the same normal vector, the non-perpendicularity has a smaller effect on the Friedel pairs at smaller Bragg angles. While the rotation axis is inclined, the center of a $\varphi - \omega$ curve moves down or up. Simultaneously, at the same Bragg angle, the positions corresponding to the four diffractions on the curve move up or down. As shown in Fig. 3, when the Bragg angle is smaller, the positions related to the Friedel pairs are closer to the center of the curve and the absolute gradients of the curve at these positions are greater; the variation of these positions in the curve to maintain the Bragg condition will correspond to smaller variation of ω, which consequently leads to smaller $\Delta\omega$. For lattice planes with the same normal vector, the effect of non-perpendicularity of the rotation axis is smaller at smaller Bragg angles.

3.2. Friedel pairs from {hkl} crystal planes

The family of {hkl} crystal planes has the same Bragg angle but different orientations. Taking the rotation axis **r** = [sin(0.01°), 0, cos(0.01°)], and the Bragg angle is 10° as an example. The values of $\Delta\omega$ related to different normal vectors on the XZ plane are shown in Table 3.

It can be seen from Table 3 that while the normal vector is closer to the XY plane the value of $\Delta\omega$ is smaller. The $\varphi(\omega)$ curves corresponding to different normal vectors are shown in Fig. 4(a). As discussed in §3.1, a greater absolute gradient corresponds to a smaller variation in ω. When the normal vector is closer to the XY plane, the absolute gradient of the $\varphi(\omega)$ curve is greater as shown in Fig. 4(b), and the rotation axis inclination leads to smaller $\Delta\omega$. The lattice planes with normal vectors closer to the XY plane will be affected less by the non-perpendicularity of the rotation axis for all {hkl} planes. The non-perpendicularity of the rotation axis has a greater effect on the lattice plane with a normal vector closer

Table 3
Rotation angles of Friedel pair A–C and angle difference $\Delta\omega$ for different normal vectors **a**.

Normal vector (**a**)	Rotation angle (A)	Rotation angle (C)	$\Delta\omega$
[sin(15°), 0, cos(15°)]	47.88°	227.78°	0.10°
[sin(30°), 0, cos(30°)]	69.69°	249.65°	0.04°
[sin(45°), 0, cos(45°)]	75.79°	255.77°	0.02°
[sin(60°), 0, cos(60°)]	78.44°	258.43°	0.01°
[sin(75°), 0, cos(75°)]	79.65°	259.64°	0.01°
[sin(90°), 0, cos(90°)]	80.00°	260.00°	0.00°

to the Z axis, and Friedel pairs from these lattice planes can be used to calculate the vector of the rotation axis.

3.3. Friedel pairs close to the XY plane

It has been indicated that a non-perpendicular rotation axis has a smaller effect on the lattice planes with normal vectors closer to the XY plane. The influence of non-perpendicularity of the rotation axis on the XZ plane on the Friedel pairs with normal vectors close to the XY plane is also investigated. Assuming that the Bragg angle is 25°, the normal vector is **a** = [sin(90°), 0, cos(90°)]. In a full 360° rotation, the angular interval is 0.01°. As shown in Table 4, the angular difference between the Friedel pair A–C increases with increasing non-
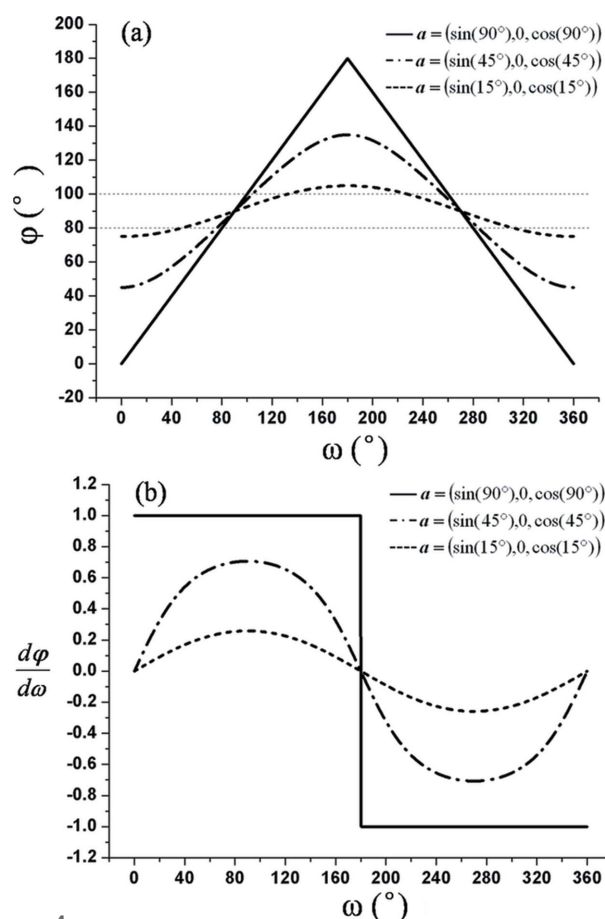
Figure 4
$\varphi(\omega)$ (a) and its gradient (b) with the rotation axis tilted by an angle of 0.01° on the XZ plane for different normal vectors.

Qiru Yi et al. • Friedel pairs and diffraction contrast tomography   **1065**

Table 4
Rotation angles of Friedel pair A–C and angle difference $\Delta\omega$ for different rotation axis vectors **r**.

Rotation axes vector (**r**)	Rotation angle (A)	Rotation angle (C)	$\Delta\omega$
$[\sin(0.01°), 0, \cos(0.01°)]$	65.01°	245.01°	0.00°
$[\sin(0.05°), 0, \cos(0.05°)]$	65.01°	245.01°	0.00°
$[\sin(0.1°), 0, \cos(0.1°)]$	65.01°	245.01°	0.00°
$[\sin(0.4°), 0, \cos(0.4°)]$	65.01°	245.01°	0.00°
$[\sin(0.6°), 0, \cos(0.6°)]$	65.01°	245.00°	0.01°
$[\sin(0.8°), 0, \cos(0.8°)]$	65.02°	244.99°	0.03°
$[\sin(1.0°), 0, \cos(1.0°)]$	65.02°	244.98°	0.04°

perpendicularity of the rotation axis, and the maximum of $\Delta\omega$ is 0.04° within a non-perpendicular angle of 1°.

Therefore, the Friedel pairs corresponding to the normal vectors which are closer to the XY plane are insensitive to the non-perpendicularity of the rotation axis. These Friedel pairs can be used to refine the setup geometry as in the case where the rotation axis is perpendicular to the incident beam (Ludwig *et al.*, 2009*b*; Reischig *et al.*, 2013). The Friedel pairs corresponding to the normal vectors which are closer to the Z axis are sensitive to the non-perpendicularity of the rotation axis. These Friedel pairs can be used to calculate the vector of the rotation axis with better precision.

4. Correct matching proportion of Friedel pairs

Under the condition that the incident X-ray direction is perfectly perpendicular to the rotation axis of a sample, the angle difference of any Friedel pair should be exactly 180°. However, when the incident X-ray direction is not perpendicular to the rotation axis, mismatch of Friedel pairs occurs, *i.e.* the angle difference of Friedel pairs will not equal 180°. Since the effect of a non-perpendicular rotation axis varies for different lattice planes as discussed above, a lattice plane with its normal vector closer to the XY plane will suffer smaller effects from the non-perpendicular rotation axis, which means smaller mismatch of Friedel pairs, while it is the opposite for the normal vector closer to the Z axis. Because the sampling angular interval is limited, a tiny effect of the non-perpendicularity of the rotation axis on lattice planes with normal vectors close to the XY plane will be difficult to observe in relevant rotation angles of diffractions. Friedel pairs from these normal vectors appear as correctly matched with an angle difference of 180°. The corresponding occupied part in the whole 4π solid angle space is defined as the correct matching district; the other part, consisting of two upward and downward cone-like spaces with opening angle 2α, is defined as the mismatching district. A sketch is shown in Fig. 5. The proportion of the correct matching district within the whole solid angle space increases when the sampling angular interval increases.

Assuming that the Bragg angle related to the normal vector **a** of a lattice plane is 20°, the proportion of the correct matching district varies for different rotation axis non-perpendicularities. When the number of grains is sufficiently large such that the orientations of a given normal vector of the
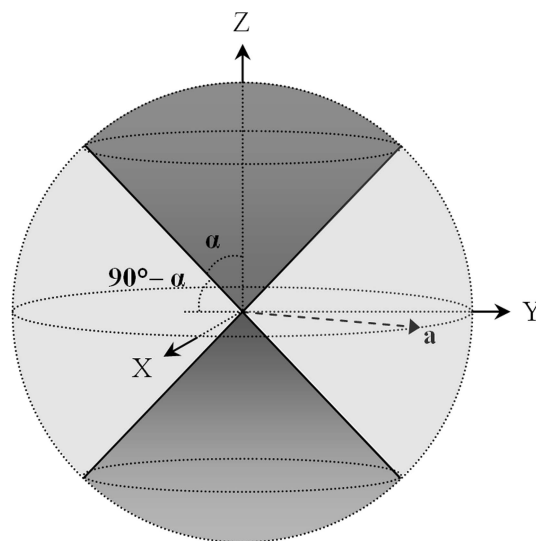
Figure 5
Sketch of the correct matching district and mismatching district in the 4π solid angle space for a given normal vector of lattice plane **a**. The space occupied by vector **a** with all possible directions is a sphere with radius of modulus **a**. The mismatching district is composed of two upward and downward spaces as shown by the darker color, each of which consists of a cone with an opening angle of 2α and a covered segment. The rest is the correct matching district. The boundary angle of these two districts is α.

lattice plane can be considered as isotropic in the whole solid angle space, the proportion will represent the correct matching proportion of the corresponding Friedel pairs. As stated in §5.1, we have used a static acquisition procedure with a sampling interval of 0.06°. Note that a diffraction spot is always expanded and spreads over several successive images for many reasons, such as the size of the grain, deformation of the lattice, X-ray energy dispersion and beam divergence. The diffraction spot may be missed in detection when the sampling angular interval exceeds the expansion, so the diffraction spot expansion is set to be 0.06° in solid angle space for calculating the matching proportions. Additionally, taking into account that the diffraction intensity has a Gaussian shape, the peak of the diffraction intensity is also likely to be missed in two successive images. We define the image which is closer to the peak of the diffraction intensity as the matched one.

Fig. 6 shows that the proportion of correct matching decreases rapidly for small non-perpendicularities (about <0.1° in this discussion), and then gradually to zero, and that a smaller sampling angular interval leads to faster falling of this proportion. The case of a Bragg angle of 10° is also calculated for comparison and the result is shown in Table 5. It indicates that the proportion of correct matching obtained from a Bragg angle of 20° is lower than that obtained from a Bragg angle of 10° at the same non-perpendicularity; thus, the decrease in the correct matching proportion of Friedel pairs caused by misalignment of the rotation axis is more severe for high-index diffractions.

For a given real object, the quantity and orientations of grains do not always satisfy the assumed condition, so the correct matching proportion of Friedel pairs from a certain family of lattice planes may not completely coincide with

Table 5
Correct matching proportion of Friedel pairs for different non-perpendicularities of the rotation axis, and different Bragg angles.

Perfect match for all orientations is represented as 1 and no match is represented as 0.

| Non- perpendicularity | Correct matching proportion | | | | | |
| | Angular interval 0.02° | | Angular interval 0.04° | | Angular interval 0.06° | |
	Bragg angle 10°	Bragg angle 20°	Bragg angle 10°	Bragg angle 20°	Bragg angle 10°	Bragg angle 20°
0.01°	0.2292	0.2216	0.5750	0.5366	0.7645	0.7320
0.02°	0.1245	0.1141	0.3567	0.3198	0.5143	0.5038
0.06°	0.0515	0.0471	0.1262	0.1245	0.2368	0.2190
0.1°	0.0323	0.0288	0.0759	0.0645	0.1201	0.1193
0.2°	0.0131	0.0096	0.0340	0.0305	0.0558	0.0523
0.7°	0	0	0	0	0.0061	0.0026
1.0°	0	0	0	0	0	0
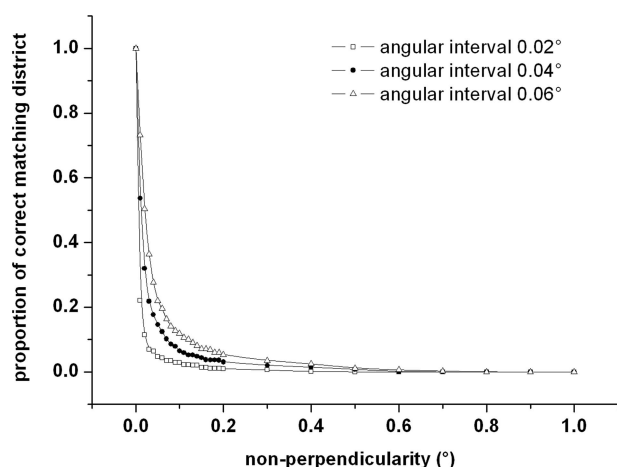
Figure 6
Proportion of the correct matching district within the 4π solid angle as a function of the non-perpendicularity of the rotation axis for different sampling angular intervals. It is assumed that the quantity of grains is sufficiently large so they are randomly oriented with respect to a given lattice plane in the whole solid angle space. The sampling angular intervals are 0.02°, 0.04° and 0.06°; the Bragg angle is 20°.

calculations at the same non-perpendicularity of the rotation axis. However, as long as the volume of the correct matching district is not zero, some normal vectors of the lattice plane can be found in this district, which could be used in geometry refinement. The choice of these normal vectors is not restricted by crystal plane family, since any normal vector of a lattice plane can appear in the correct matching district because the orientation of the grain could be in any direction. In fact, owing to a limited sampling angular interval and a specific choice of rotating start, the boundary between the correct matching district and the mismatching district is not as sharp as shown in Fig. 5. For simplicity, we defined the degree of the boundary angle α as the mid-value of the smallest angle where the correctly matched Friedel pairs can be observed and the largest angle where the mismatched Friedel pairs can be observed. For a family of lattice planes with Bragg angle of 20°, the degree of the boundary angle α as a function of the non-perpendicularity for different sampling angular intervals is shown in Fig. 7.

Fig. 7 shows that the boundary angle increases rapidly when the rotation axis inclines by about 0.1° and then gradually to 90°; the correct matching district will reduce and even disappear. The smaller sampling angular interval corresponds to a smaller non-perpendicularity limit where the correct matching district disappears. However, the Friedel pairs from the normal vectors of the lattice plane close to the *XY* plane is a good starting point for geometry refinement due to its highest correct matching possibility before the non-perpendicularity of the rotation axis is determined.

5. Experiment and discussion

5.1. Experiment setup

The DCT experiment was performed at the imaging beamline 4W1A of Beijing Synchrotron Radiation Facility (BSRF). The sample was a pure aluminium cylinder with a diameter of about 700 µm and a mean grain size of about 500 µm. The X-ray energy was about 20 keV, obtained by a double Si (111) monochromator, and the field of view was limited to 1.3 mm × 1.3 mm by slits. The two-dimensional X-ray detector was a high-resolution X-ray imaging system (M11427-42) with an ORCA-Flash4.0 scientific CMOS camera (Hamamatsu Photonics) containing 2048 × 2048 pixels. The pixel size was 6.5 µm × 6.5 µm, and the dynamic range was
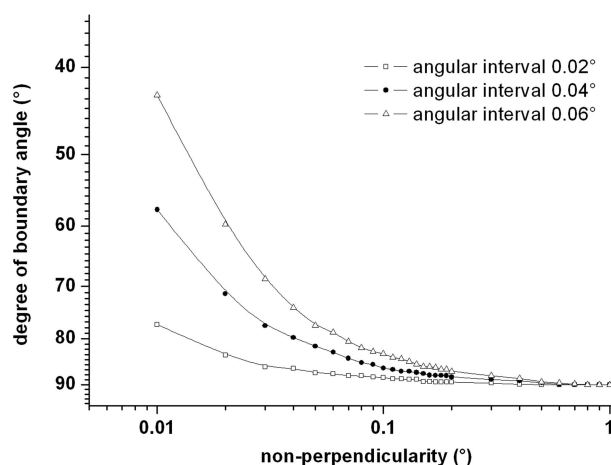
Figure 7
The boundary angle α between the correct matching district and mismatching district as a function of non-perpendicularity of the rotation axis for different sampling angular intervals. The Bragg angle is 20°.
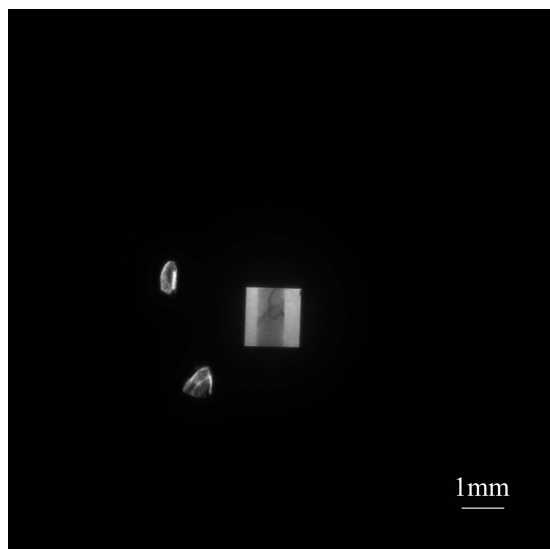
Figure 8
A typical image in a DCT experiment performed at beamline 4W1A, BSRF. The X-ray energy was about 20 keV, and exposure time was 3 s.

16-bit. The object was rotated in full 360°, and 6000 images were acquired in a static scanning procedure with a step of 0.06° (3 s exposures for each image) in the experiment.

5.2. Experiment results

A total of 1624 diffraction spots below (400), related to 406 lattice planes, were found in the experiment data, excluding those beyond the detector or diffractions that did not occur because the normal of the lattice plane was too close to the rotation axis. One image is shown in Fig. 8 as an example. The analysis of the experiment data indicates that when the normal vector of the lattice plane is close to the XY plane the Friedel pairs match well the rotation angle difference of 180°, whereas when the normal vector is close to the Z axis this difference deviates from 180° and even becomes 0.9°. The correct matching proportion of Friedel pairs is only 18.7%. This means a notable perpendicularity deflection of the rotation axis.

The predicted and actual diffraction angles (or image numbers) for grain A in Fig. 9 are listed in Appendix A as an example. This shows that, for the same Bragg angle, non-perpendicularity of the rotation axis has greater effects on the Friedel pairs with normal vector closer to the Z axis. For example, the relevant rotation angles of the Friedel pair from $(-1-11)$ with the normal vector close to the XY plane are 117.78° and 297.78°, respectively, and the rotation angle difference is 180°. On the other hand, the Friedel pair from $(1-11)$ with the normal vector close to the Z axis appears at rotation angles of 17.04° and 197.58°, and the rotation angle difference is 180.54°. The result also shows that non-perpendicularity of the rotation axis has smaller effects on the Friedel pairs at smaller Bragg angles. For instance, the rotation angle corresponding to the $(1-11)$ Friedel pair is 180.54°, while that corresponding to the $(2-22)$ Friedel pair is 180.66°. These results are consistent with the analysis in §3.
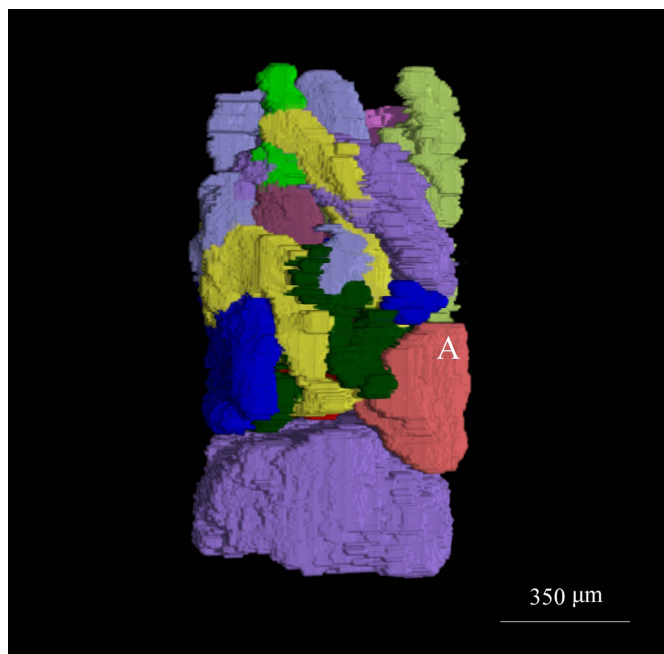
Figure 9
Three-dimensional reconstruction of the aluminium sample with 13 grains. Some grains are not rendered in this view angle. The image numbers corresponding to the diffractions from grain A are listed in Appendix A. Color coding of the grains is based on the angle between its normal vectors of (0 0 2) and the Z axis.

The initial indexing was performed with diffraction spots close to the XY plane using the method introduced by Ludwig and co-workers (Ludwig *et al.*, 2009*b*; Reischig *et al.*, 2013). The X-ray energy was modified to 20.04 keV, and then 2θ can be obtained with the modified energy. Combining with the values of 2θ and positions of Friedel pairs on the XY plane, the sample-to-detector distance was obtained to be 8.67 ± 0.01 mm. The normal vector of the diffractive lattice plane close to the Z axis is deduced from an extinction–diffraction spot pair (Johnson *et al.*, 2008). Utilizing ω and φ of a Friedel pair close to the Z axis and the constraint $|\mathbf{r}| = 1$, the rotation axis was determined from equation (4) as $\mathbf{r} = (0.0018, 0.0357, 0.9994)$, and its deviation from the perpendicularity is 0.10°.

It should be indicated that an extinction–diffraction spot pair is needed to confirm the initial normal vector close to the Z axis for calculating the rotation axis orientation, and matching and indexing other diffraction spots can be deduced after the rotation axis is determined. However, choosing this extinction–diffraction spot pair is expected to be more difficult when a sample contains thousands of grains or has higher levels of intragranular orientation spread. The normal vector close to the Z axis can be acquired *via* combining the diffraction spots close to the XY plane from the same grain if they simultaneously appear on one image, and an alternative approach called the forward modeling method (Suter *et al.*, 2006) is hoped to solve this problem.

In the experiment the smallest and largest Bragg angles of the collected diffractions are 7.6° and 17.79°, corresponding to (111) and (400), respectively. At a non-perpendicularity

of 0.10°, the calculated boundary angles between correct matching and mismatching regions of Friedel pairs of the two families are 83.00° and 83.15° for a sampling angular interval of 0.06°. Experiment results show that, for all the normal vectors in the correct matching district, the angles between the normal vectors and the Z axis are located in the range 83.23–89.76°, consistent with the calculations.

Collected diffraction spots from the sample can be classified into 13 groups based on 13 grains. All the positions and corresponding rotation angles of the diffraction spots below (400) were calculated using the refined geometric parameters including the rotation axis. The mismatch in image numbers between calculation and experiment is only within two images, and 90.62% of the actual images are in complete agreement with the calculation. If the rotation axis is taken as perfectly aligned, the proportion of matching Friedel pairs is only 18.7%. The improvement of the correct matching and indexing proportion of diffraction spots can improve the calculation of diffracted beam paths and increase the number of valid pairs for recovery of shape and location of grain. Thus, the method presented above is applicable to the case of a non-perpendicular rotation axis. The calculated image numbers for diffractions from grain A are compared with the actual image numbers in Appendix A.

Three-dimensional reconstruction of the sample was performed using the ART method and the result is shown in Fig. 9. The sample displayed has a length of about 1.2 mm and a diameter of ~700 μm. The largest grain is about 700 μm at the bottom and the smallest one is about 200 μm as calculated from the reconstruction.

5.3. Discussions

The experiment result shows that the correct matching proportion of the actual image numbers to the calculated image numbers is 90.62% instead of 100%. The main mismatch comes from the Friedel pairs which are sensitive to the non-perpendicularity of the rotation axis. It can be seen from equation (4) that the orientation precision of the rotation axis $\mathbf{r}$ corresponds to the precision of ω and orientation of normal vector $\mathbf{a}$. A smaller rotation angular interval of ω can yield a more accurate rotation axis. However, the orientation precision of the rotation axis is limited due to the limit in the rotation angle step, leading to mismatches in the Friedel pairs sensitive to the non-perpendicular rotation axis.

Although it is difficult for the rotation axis to be perfectly perpendicular to the incident X-ray direction in practice, Friedel pairs may match well in the situation of small non-perpendicularity of the rotation axis with relative large tolerance interval. The misalignment of the rotation axis could be ignored in such cases. However, the peak of diffraction intensity may be missed with relatively large sampling angular intervals. A smaller sampling angular interval should lead to more precise searching of the intensity peak which can be used to determine the diffraction geometry with higher precision and consequently improve the reconstructive precision of grains.

When a polycrystalline sample contains of the order of 10^2–10^3 grains, diffraction spots will significantly increase, and some spots from other grains may appear in the 180° offset image due to misalignment, probably leading to errors in matching Friedel pairs. On the other hand, given the limited detector size, diffraction spots from different (hkl) families in a large number of grains may not be sufficiently separated on the detector. Both of the problems can be expected to cause difficulties in the initial selection of a Friedel pair close to the XY plane, so the tolerance for the pair selection has to be reduced to ensure correct pairing, and grains can only be partially indexed and reconstructed in the 3D grain map.

Three-dimensional reconstruction of grains using the ART method is based on the paths of the diffracted beam. Refinement of the experimental geometry and determination of the rotation axis could improve the orientation precision of the diffraction beam for higher precision in determining the shapes and locations of the reconstructed grains. However, with this method it is difficult to eliminate the effect of energy dispersion and beam divergence; on the other hand, the data processing method presented here mainly depends on the precise determination of Friedel pairs. Combining with the forward modeling method (Suter *et al.*, 2006) promises to overcome these problems to improve the precision of the geometry refinement and grain reconstruction.

It should be noted that analysis in this work is focused on the rotation axis inclination on the XZ plane. In fact, the inclination may also occur in the YZ plane. The angle between the X-ray incident direction and the rotation axis maintains 90° when the rotation axis inclines on the YZ plane, so it has no effect on the discrepancy of the rotation angle between the two diffractions in a Friedel pair, and only positions of diffraction spots on a two-dimensional detector will be changed. It is essentially the ordinary DCT geometric setup. The significant effects are caused by the rotation axis inclined on the XZ plane as discussed above.

6. Conclusion

We have presented detailed analysis of the characteristics of Friedel pairs in the condition that the rotation axis of a sample is not exactly perpendicular to the X-ray incident direction regarding DCT. The Friedel pairs close to the XY plane are insensitive to the non-perpendicularity of the rotation axis, and can be used as a good starting point to refine the sample-to-detector distance and X-ray energy; the Friedel pairs close to the Z axis are sensitive to this non-perpendicularity, and can be used to determine the rotation axis orientation. The correct matching proportion of Friedel pairs decreases with increasing non-perpendicularity of the rotation axis, and this reduction may undermine matching and indexing of diffraction spots based on Friedel pairs. Precise determination of the rotation axis orientation can increase the correct matching and indexing proportions of diffraction spots, and thus improves the reconstruction precision of grains. The experiment on an aluminium polycrystalline sample was performed at BSRF with a non-perpendicular angle of 0.10°. If the rotation axis is

taken as perfectly aligned, the proportion of matching Friedel pairs is only 18.7%. However, the calculation of diffraction spots collectable from the sample with determined rotation axis showed high correspondence with the experiment data with up to about 90.62% correct proportion. This method was successfully applied to 3D reconstruction of the sample, demonstrating that the method is applicable to DCT suffering from misalignment of the rotation axis.

APPENDIX A

A comparison between the predicted and actual image numbers for diffractions from grain A is given in Table 6.

Table 6
Comparison between the predicted (P) and actual (A) image numbers for diffractions from grain A.

The rotation angle interval is 0.06°. The rotation angle is image number × 0.06°. In the experiment, the first six families [(111) to (004)] of the sample can be observed on the detector. We have 124 diffraction spots [diffraction of (202) does not occur] and a maximum of 62 Friedel pairs. Only eight actual images have a mismatch to the prediction (marked in bold). About 93.55% of the actual images are accurately consistent with the calculation. The four image numbers correspond to diffraction spots A, B, C and D as mentioned in §3. $\Delta\omega$ is used to represent the difference between $\omega_C - \omega_A$ and 180°, and γ is the angle between the normal vector and the Z axis. The table shows that, for the same Bragg angle, the smaller value of γ, meaning that the normal vector is closer to the Z axis, corresponds to a greater absolute value of $\Delta\omega$. The result also shows that non-perpendicularity of the rotation axis has smaller effects on the Friedel pairs corresponding to smaller Bragg angles. For the Friedel pairs located in the correct matching district, the minimum of γ is 83.23° and the maximum of γ is 88.66°, which is consistent with the calculations.

Plane index	θ (°)		A	B	C	D	$\Delta\omega$ (°)	γ (°)
(1 −1 1)	7.604	P:	0284	2649	3293	5641	0.54	25.43
		A:	0284	2649	3293	5641		
(1 1 1)	7.604	P:	0207	2856	3204	5859	−0.18	45.15
		A:	0207	2856	3204	5859		
(1 −1 −1)	7.604	P:	0805	1061	3805	4061	0	83.23
		A:	0805	1061	3805	4061		
(−1 −1 1)	7.604	P:	1963	2217	4963	5217	0	85.41
		A:	1963	2217	4963	5217		
(2 0 0)	8.793	P:	1498	1915	4502	4918	0.24	44.53
		A:	1498	1915	4502	4918		
(0 0 2)	8.793	P:	**1127**	1527	4123	4523	−0.18	47.16
		A:	**1126**	1527	4123	4523		
(0 −2 0)	8.793	P:	0158	2859	3159	5859	0.06	80.14
		A:	0158	2859	3159	5859		
(2 0 2)	12.486	P:		No diffraction				9.97
		A:		No diffraction				
(2 −2 0)	12.486	P:	0396	0943	3399	3946	0.18	51.30
		A:	0396	0943	3399	3946		
(0 −2 2)	12.486	P:	2064	2599	5061	5596	−0.18	52.99
		A:	2064	2599	5061	5596		
(2 2 0)	12.486	P:	2259	2705	5260	5706	0.06	67.49
		A:	2259	2705	5260	5706		
(0 2 2)	12.486	P:	**0335**	0777	**3334**	3776	−0.06	68.92
		A:	**0336**	0777	**3335**	3776		
(2 0 −2)	12.486	P:	1305	1721	4305	4721	0	88.66
		A:	1305	1721	4305	4721		
(3 −1 1)	14.678	P:	0621	1840	3630	**4849**	0.54	25.64
		A:	0621	1840	3630	**4850**		
(1 −1 3)	14.678	P:	1217	2327	4209	5319	−0.48	28.15
		A:	1217	2327	4209	5319		
(3 1 1)	14.678	P:	1924	2724	4928	5729	0.24	37.04
		A:	1924	2724	4928	5729		

Table 6 (continued)

Plane index	θ (°)		A	B	C	D	$\Delta\omega$ (°)	γ (°)
(1 1 3)	14.678	P:	0352	1124	3348	4119	−0.24	38.89
		A:	0352	1124	3348	4119		
(1 −3 1)	14.678	P:	0304	2691	3307	5688	0.18	54.91
		A:	0304	2691	3307	5688		
(3 −1 −1)	14.678	P:	0997	1563	3999	4565	0.12	60.57
		A:	0997	1563	3999	4565		
(−1 −1 3)	14.678	P:	1464	2017	4462	5015	−0.12	63.15
		A:	1464	2017	4462	5015		
(3 1 −1)	14.678	P:	**1653**	2182	**4655**	5183	0.12	67.16
		A:	**1655**	2182	**4656**	5183		
(−1 1 3)	14.678	P:	0854	1375	3853	4374	−0.06	69.60
		A:	0854	1375	3853	4374		
(1 3 1)	14.678	P:	0270	2765	3269	5766	−0.06	74.63
		A:	0270	2765	3269	5766		
(1 3 −1)	14.678	P:	0188	0687	3189	3688	0.06	80.51
		A:	0188	0687	3189	3688		
(−1 −3 1)	14.678	P:	2333	2830	5332	5829	−0.06	81.66
		A:	2333	2830	5332	5829		
(2 −2 2)	15.346	P:	**0652**	2282	**3663**	5271	0.66	25.43
		A:	**0653**	2282	**3664**	5271		
(2 2 2)	15.346	P:	0387	2676	3383	5680	−0.24	45.15
		A:	0387	2676	3383	5680		
(2 −2 −2)	15.346	P:	0675	1191	3675	4191	0	83.23
		A:	0675	1191	3675	4191		
(−2 −2 2)	15.346	P:	1833	2347	4833	5347	0	85.41
		A:	1833	2347	4833	5347		
(4 0 0)	17.794	P:	1280	2133	4283	5137	0.18	44.53
		A:	1280	2133	4283	5137		
(0 0 4)	17.794	P:	0918	1736	3914	4733	−0.24	47.16
		A:	0918	1736	3914	4733		
(0 −4 0)	17.794	P:	0312	2706	3312	5705	0	80.14
		A:	0312	2706	3312	5705		

References

Bernier, J. V., Barton, N. R., Lienert, U. & Miller, M. P. (2011). *J. Strain Anal. Engineering Des.* **46**, 527–547.
Cloetens, P., Pateyron-Salomé, M., Buffière, J. Y., Peix, G., Baruchel, J., Peyrin, F. & Schlenker, M. (1997). *J. Appl. Phys.* **81**, 5878–5886.
Herbig, M., King, A., Reischig, P., Proudhon, H., Lauridsen, E. M., Marrow, J., Buffière, J. & Ludwig, W. (2011). *Acta Mater.* **59**, 590–601.
Johnson, G., King, A., Honnicke, M. G., Marrow, J. & Ludwig, W. (2008). *J. Appl. Cryst.* **41**, 310–318.
King, A., Herbig, M., Ludwig, W., Reischig, P., Lauridsen, E. M., Marrow, T. & Buffière, J. (2010). *Nucl. Instrum. Methods Phys. Res. B*, **268**, 291–296.
King, A., Johnson, G., Engelberg, D., Ludwig, W. & Marrow, J. (2008). *Science*, **321**, 382–385.
King, A., Ludwig, W., Herbig, M., Buffière, J., Khan, A. A., Stevens, N. & Marrow, T. J. (2011). *Acta Mater.* **59**, 6761–6771.
Kostenko, A., Sharma, H., Dere, E. G., King, A., Ludwig, W., Oel, W., Offerman, S. E., Stallinga, S. & Vliet, L. J. (2012). *AIP Conf. Proc.* **1437**, 63–68.

Lauridsen, E. M., Schmidt, S., Suter, R. M. & Poulsen, H. F. (2001). *J. Appl. Cryst.* **34**, 744–750.

Li, S. F. & Suter, R. M. (2013). *J. Appl. Cryst.* **46**, 512–524.

Ludwig, W., King, A., Herbig, M., Reischig, P., Marrow, J., Babout, L., Lauridsen, E. M., Proudhon, H. & Buffière, J. Y. (2010). *JOM*, **62**, 22–28.

Ludwig, W., King, A., Reischig, P., Herbig, M., Lauridsen, E. M., Schmidt, S., Proudhon, H., Forest, S., Cloetens, P., du Roscoat, S. R., Buffière, J. Y., Marrow, T. J. & Poulsen, H. F. (2009a). *Mater. Sci. Eng. A*, **524**, 69–76.

Ludwig, W., Reischig, P., King, A., Herbig, M., Lauridsen, E. M., Johnson, G., Marrow, T. J. & Buffière, J. Y. (2009b). *Rev. Sci. Instrum.* **80**, 033905.

Ludwig, W., Schmidt, S., Lauridsen, E. M. & Poulsen, H. F. (2008). *J. Appl. Cryst.* **41**, 302–309.

Moscicki, M., Kenesei, P., Wright, J., Pinto, H., Lippmann, T., Borbély, A. & Pyzalla, A. (2009). *Mater. Sci. Eng. A*, **524**, 64–68.

Nervo, L., King, A., Wright, J. P., Ludwig, W., Reischig, P., Quinta da Fonseca, J. & Preuss, M. (2014). *J. Appl. Cryst.* **47**, 1402–1416.

Peetermans, S. & Lehmann, E. H. (2013). *J. Appl. Phys.* **114**, 124905.

Reischig, P., King, A., Nervo, L., Viganó, N., Guilhem, Y., Palenstijn, W. J., Batenburg, K. J., Preuss, M. & Ludwig, W. (2013). *J. Appl. Cryst.* **46**, 297–311.

Schmidt, S. (2005). *GrainSweeper*, http://fable.svn.sourceforge.net/svnroot/fable/GrainSweeper.

Schmidt, S. (2014). *J. Appl. Phys.* **47**, 276–284.

Sharma, H., Huizenga, R. M. & Offerman, S. E. (2012). *J. Appl. Cryst.* **45**, 705–718.

Suter, R. M., Hennessy, D., Xiao, C. & Lienert, U. (2006). *Rev. Sci. Instrum.* **77**, 123905.

Syha, M., Rheinheimer, W., Bäurer, M., Lauridsen, E. M., Ludwig, W., Weygand, D. & Gumbsch, P. (2012). *Scr. Mater.* **66**, 1–4.

Syha, M., Trenkle, A., Lödermann, B., Graff, A., Ludwig, W., Weygand, D. & Gumbsch, P. (2013). *J. Appl. Cryst.* **46**, 1145–1150.